

# Multi-view MERA Subspace Clustering

Zhen Long\*, Ce Zhu\*, Jie Chen\*, Zihan Li\*, Yazhou Ren<sup>†</sup>, Yipeng Liu \*

May 17, 2023

## Abstract

Tensor-based multi-view subspace clustering (MSC) can capture high-order correlation in the self-representation tensor. Current tensor decompositions for MSC suffer from highly unbalanced unfolding matrices or rotation sensitivity, failing to fully explore inter/intra-view information. Using the advanced tensor network, namely, multi-scale entanglement renormalization ansatz (MERA), we propose a low-rank MERA based MSC (MERA-MSC) algorithm, where MERA factorizes a tensor into contractions of one top core factor and the rest orthogonal/semi-orthogonal factors. Benefiting from multiple interactions among orthogonal/semi-orthogonal (low-rank) factors, the low-rank MERA has a strong representation power to capture the complex inter/intra-view information in the self-representation tensor. The alternating direction method of multipliers is adopted to solve the optimization model. Experimental results on five multi-view datasets demonstrate MERA-MSC has superiority against the compared algorithms on six evaluation metrics. Furthermore, we extend MERA-MSC by incorporating anchor learning to develop a scalable low-rank MERA based multi-view clustering method (sMERA-MVC). The effectiveness and efficiency of sMERA-MVC have been validated on three large-scale multi-view datasets. To our knowledge, this is the first work to introduce MERA to the multi-view clustering topic. The codes of MERA-MSC and sMERA-MVC are publicly available at <https://github.com/longzhen520/MERA-MSC>.

## 1 Introduction

Multi-view data are ubiquitous in the real world. For instance, certain news can be reported in text, images, and video; the multi-view Yale database can be represented by local binary patterns (LBP), Gabor, and intensity features. Such multi-view data, which provide consensual and complementary information, have given rise to a series of multi-view learning based tasks [34, 50, 56].

---

\*Z. Long, C. Zhu, J. Chen, Z. Li and Y. Liu are with the School of Communication and Information Engineering, and University of Electronic Science and Technology of China (UESTC), Chengdu 611731, China. (email: [eczhu@uestc.edu.cn](mailto:eczhu@uestc.edu.cn); [yipengliu@uestc.edu.cn](mailto:yipengliu@uestc.edu.cn))

<sup>†</sup>Y. Ren is with the School of Computer Science and Engineering, UESTC, Chengdu, 611731, China.

Among them, multi-view subspace clustering (MSC) separates multi-view data into several groups by assuming it shares a common latent low-dimensional subspace, driving numerous applications in image processing and computer vision [29, 31, 43, 46, 48].

Inspired by the success of low-rank representation (LRR) [38] and sparse subspace clustering (SSC) [8] on single-view data, where each sample can be represented by a combination of other samples, many self-representation based MSC methods have been proposed. Among them, tensor-based MSC ones show promising performances by assuming that their self-representation tensors are low-rank [6, 10, 49, 53]. For example, Zhang et al. [53] firstly stack all subspace representations of each view to a 3rd-order tensor and consider Tucker low-rank constraint [23] on it to explore the high-order correlations among views. However, Tucker nuclear norm is denoted as the sum of the nuclear norms of the unfolding matrices, which captures the low-rank information from unbalanced unfolding matrices, resulting in inferior performance [2, 49]. To alleviate it, Xie et al. [49] consider the tubal norm based on tensor singular value decomposition (t-SVD) [18] for low-rank self-representation tensor, where the tensor is rotated to effectively capture the consensus among multiple views.

However, the self-representation tensor contains both inter- and intra-view similarity information. For t-SVD, the rotation operation of the self-representation tensor can well explore the correlations across different views, but it also suffers from inadequate exploration of intra-view information, because matrix singular value decompositions (SVDs) are only performed in the first two modes, and linear transformations are considered in the third mode [24–26]. On account of these, Jia et al. [15] introduce low-rankness to the frontal and the horizontal slices of the self-representation tensor to characterize the intra-view and inter-view relationships, respectively. On exploring inter/intra-view information in the self-representation tensor, one question naturally arises: whether the inter/intra-view information can be well captured simultaneously with a new tensor decomposition. In fact, as advanced tensor decompositions, tensor networks show significant advantages in capturing the correlation of higher order data [2, 27, 42].

In this paper, we consider a stable tensor network, namely the multi-scale entanglement renormalization ansatz (MERA) decomposition [1, 37, 51], to capture well both inter- and intra-view information of the self-representation tensor. MERA factorizes a  $D$ -th order tensor into several orthogonal/semi-orthogonal factors and one top core factor, providing a more expressive and powerful representation of a high-order tensor. To make it clear, Fig. 1 provides the reconstructed images obtained by different tensor decompositions, including t-SVD, Tucker decomposition, and MERA decomposition, under the same compression ratio (CR), i.e., CR=5%. From Fig. 1(b-d), it is evident that the low-rank MERA approximation exhibits better recovery performance in terms of PSNR than the other approximation methods. This implies that MERA has a more powerful representation capability in comparison to t-SVD and Tucker decomposition.

Based on it, we develop a low-rank MERA-based MSC (MERA-MSC) opti-

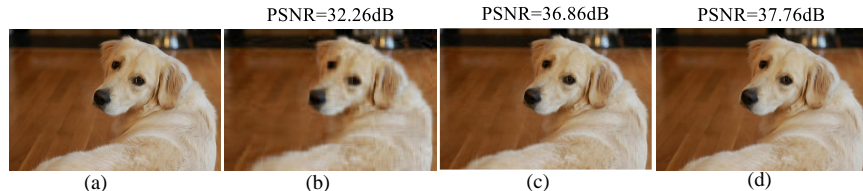


Fig. 1. Low-rank exploration performance of t-SVD, Tucker, and MERA on RGB image at the same 5% compression ratio; (a) is the original image with size  $640 \times 960 \times 3$ ; The images in (b)-(d) correspond to the recovered images obtained by low-rank t-SVD approximation, low-rank Tucker approximation, and low-rank MERA approximation, respectively.

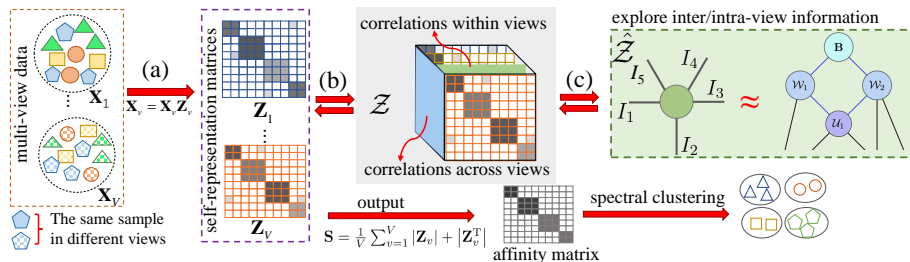


Fig. 2. Framework of MERA-MSC. Each data  $\mathbf{X}_v$  can be first expressed with its linear combination, e.g., (a)  $\mathbf{X}_v = \mathbf{X}_v \mathbf{Z}_v$ ; (b) these self-representation matrices  $\mathbf{Z}_v, v = 1, \dots, V$  are stacked into a self-representation tensor  $\mathcal{Z}$ ; (c)  $\mathcal{Z}$  will be reshaped into a 5-th order tensor, on which low-rank MERA approximation is performed to capture both inter- and intra-view correlations. In each iteration,  $\mathbf{Z}_v$  is adaptively obtained from both  $\mathbf{X}_v$  and the updated  $\hat{\mathbf{Z}}_v$  from low-rank MERA approximation. At last, the affinity matrix can be constructed by  $\frac{1}{V} \sum_{v=1}^V |\mathbf{Z}_v| + |\mathbf{Z}_v^T|$ , which will then be fed into the spectral clustering algorithm.

mization model, and the alternating direction method of multipliers (ADMM) framework [3] is adopted to solve it. The processing of MERA-MSC is illustrated in Fig. 2, where the self-representation tensor will be adaptively updated from the multi-view data and low-rank MERA approximation in each iteration. Iteratively, the final self-representation tensor will be used to construct the affinity matrix, which will then be fed into the spectral clustering algorithm [39] for achieving MSC task. Furthermore, we extend the MERA-MSC method using anchor learning and developed a scalable MERA based multi-view clustering (sMERA-MVC) algorithm in the experimental part.

Our contributions are summarized as follows:

- Motivated by the powerful representation ability of MERA decomposition, we apply it to capture the inter/intra-view correlations within the self-representation tensor for MSC. To the best of our knowledge, this is the

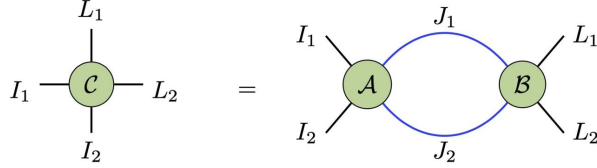


Fig. 3. The graphical illustration of tensor contraction.

first work to introduce MERA to MVC tasks.

- An effective algorithm named MERA-MSC is proposed and evaluated on five benchmark datasets. Experimental results show MERA-MSC outperforms the state-of-art methods, as evaluated using six commonly used metrics. Building upon this, an sMERA-MVC is further developed, which clusters large-scale multi-view data effectively and efficiently.
- The outstanding clustering performance of MERA-MSC and sMERA-MVC highlights the capability of low-rank MERA approximation to explore higher-order correlation, which also provides some inspiration for applying it to other tasks, like tensor classification, tensor regression.

## 2 NOTATIONS AND PROBLEM FORMULATION

### 2.1 Notations

A scalar, a vector, a matrix, and a tensor are written as  $x$ ,  $\mathbf{x}$ ,  $\mathbf{X}$ , and  $\mathcal{X}$ , respectively. Indices typically range from 1 to their capital version, e.g.,  $i = 1, \dots, I$ . For a  $D$ -th order tensor  $\mathcal{X} \in \mathbb{R}^{I_1 \times \dots \times I_D}$ , its mode- $\{d_1, d_2\}$  unfolding matrix is represented as  $\mathbf{X}_{(d_1, d_2)} \in \mathbb{R}^{I_{d_1} I_{d_2} \times \prod_{e \neq d_1, d_2} I_e}$  by arranging the  $\{d_1, d_2\}$ -th mode of  $\mathcal{X}$  as the row while the rest modes as the column, and its inverse operator is defined by  $\mathcal{X} = \text{fold}_{d_1, d_2}(\mathbf{X}_{(d_1, d_2)})$ . As shown in Fig. 3, the tensor contraction of two tensors  $\mathcal{A} \in \mathbb{R}^{I_1 \times I_2 \times J_1 \times J_2}$  and  $\mathcal{B} \in \mathbb{R}^{J_1 \times J_2 \times L_1 \times L_2}$  is achieved by contracting their common indices  $\{J_1, J_2\}$ , which is denoted as  $\mathcal{C} = \mathcal{A} \times_{\{J_1, J_2\}} \mathcal{B} \in \mathbb{R}^{I_1 \times I_2 \times L_1 \times L_2}$  whose entries are calculated by  $c_{i_1, i_2, l_1, l_2} = \sum_{j_1, j_2} a_{i_1, i_2, j_1, j_2} b_{j_1, j_2, l_1, l_2}$ .

### 2.2 MERA Decomposition

Before introducing the MERA decomposition, it is necessary to introduce two fundamental building blocks: isometry and disentangler.

**Definition 1** (Isometry). [1, 37] As shown in Fig. 4(a), an isometry  $\mathcal{W} \in \mathbb{R}^{I_1 \times \dots \times I_K \times R}$  is denoted as a  $(K+1)$ -th order tensor with semi-orthogonal unfolding matrix  $\mathbf{W} \in \mathbb{R}^{I_1 \dots I_K \times R}$ , e.g.,  $\mathbf{W}^T \mathbf{W} = \mathbf{I}_R$ , where  $R$  is the outgoing dimension of an isometry and  $K$  is the number of bottom legs.

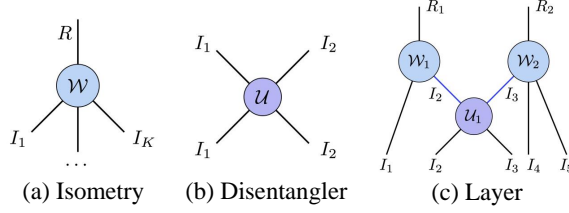


Fig. 4. The graphical representations of isometry, disentangler, and layer, respectively.

**Definition 2** (Disentangler). [1, 37] As shown in Fig. 4(b), a disentangler  $\mathcal{U} \in \mathbb{R}^{I_1 \times I_2 \times I_1 \times I_2}$  is denoted as a 4-way tensor with a square orthogonal unfolding matrix  $\mathbf{U} \in \mathbb{R}^{I_1 I_2 \times I_1 I_2}$ , namely,  $\mathbf{U}^T \mathbf{U} = \mathbf{I}_{I_1 I_2}$ .

**Definition 3** (Layer). [1, 37] A layer  $\mathcal{C}$  is denoted as a result of tensor contraction between isometries and disentanglers in the same layer. For example, as shown in Fig. 4(c), a 7-th order layer  $\mathcal{C}$  can be constructed by two isometries  $\mathcal{W}_1 \in \mathbb{R}^{I_1 \times I_2 \times R_1}$ ,  $\mathcal{W}_2 \in \mathbb{R}^{I_3 \times I_4 \times I_5 \times R_2}$  and one disentangler  $\mathcal{U} \in \mathbb{R}^{I_2 \times I_3 \times I_2 \times I_3}$ , as follows:

$$\mathcal{C} = \mathcal{U}_1 \times_{\{I_2\}} \mathcal{W}_1 \times_{\{I_3\}} \mathcal{W}_2 \in \mathbb{R}^{I_1 \times I_2 \times I_3 \times I_4 \times I_5 \times R_1 \times R_2}.$$

**Definition 4** (MERA Decomposition). [1, 37] For a  $D$ -th order tensor  $\mathcal{Z} \in \mathbb{R}^{I_1 \times I_2 \times \dots \times I_D}$ , its MERA representation can be composed by different layers and one top core, which can be recursively obtained by:

$$\mathcal{G}^{l-1} = \mathcal{G}^l \times_{\{R_1^l, \dots, R_{P_l}^l\}} \mathcal{C}_l, \quad (1)$$

where  $R_{p_l}^l, p_l = 1, \dots, P_l, l = 1, \dots, L$  are the MERA ranks;  $P_l$  is the number of isometries in  $l$ -th layer, and  $L$  is the total number of layers.  $\mathcal{G}^0 = \mathcal{Z}$ , and  $\mathcal{G}^L = \mathbf{B}$ , where  $\mathbf{B}$  is the top core. In a nested way, we can construct the MERA decomposition.

For simplification, we use  $\mathcal{Z} = f(\mathbf{B}, \mathcal{W}, \mathcal{U})$  to represent an MERA decomposition, where  $\mathcal{U} = (\mathcal{U}_1^l, \dots, \mathcal{U}_{P_l-1}^l)$  and  $\mathcal{W} = (\mathcal{W}_1^l, \dots, \mathcal{W}_{P_l}^l)$ ,  $\mathcal{W}_{p_l}^l$  and  $\mathcal{U}_{p_l}^l$  are the  $p_l$ -th isometry and disentangler in the  $l$ -th layer,  $l = 1, \dots, L$ . Fig. 5 shows the graphical representation of MERA decomposition for a 5-th order tensor.

## 2.3 Related Works

According to different representation forms of self-representation matrices in multi-view data, current MSC methods are mainly divided into two categories: one is matrix-based MSC, which learns a shared self-representation matrix of all views; the other is tensor-based MSC, which stacks self-representation matrices of all views into a tensor to explore the correlations among views.

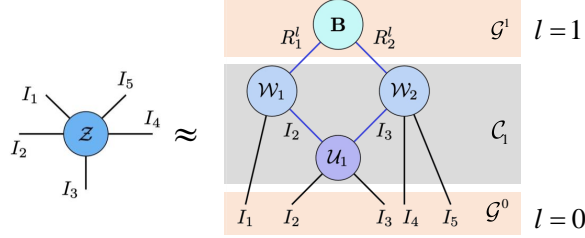


Fig. 5. An graphical illustration of MERA decomposition for a 5-th order tensor.

### 2.3.1 Matrix-based MSC

Current matrix-based MSC methods generally consider that multi-view data possess a shared consistent feature while each view has its specific feature that provides complementary information, namely consistency and diversity [20, 43]. Specifically, [43] considers a shared indicator matrix and a position-aware exclusivity term as the consistent and the diversity representations, respectively. [28] divides the self-representation matrix of each view into two parts: the low-rank consensus shared by all views and the specific part of every single view constrained by  $\ell_2$  norm. Furthermore, instead of the original space, [57] projects multi-view data into a latent space to exploit shared-specific information. Besides, [32] considers the interaction between the learned self-representation and the clustering calculation and proposes a unified MSC framework to learn a better subspace self-representation for clustering.

### 2.3.2 Tensor based MSC

Tensor-based MSC methods can well capture high-order correlations among multiple views, showing improved clustering performance [35, 53]. The key idea of tensor-based MSC methods is to find a good low-rank tensor approximation for the self-representation tensor. Given multi-view dataset  $\mathbf{X}_v \in \mathbb{R}^{D_v \times N}$ ,  $v = 1, \dots, V$ , where  $V$  and  $N$  are the numbers of views and samples, respectively, and  $D_v$  represents the feature dimension in the  $v$ -th view. The general tensor-based MSC optimization model can be formulated as [53]:

$$\begin{aligned}
 & \min_{\{\mathbf{E}_v, \mathbf{Z}_v\}_{v=1}^V} \Phi(\mathcal{Z}) + \lambda \Psi(\mathbf{E}) \\
 \text{s. t. } & \mathbf{X}_v = \mathbf{X}_v \mathbf{Z}_v + \mathbf{E}_v, v = 1, \dots, V, \\
 & \mathcal{Z} = \Omega(\mathbf{Z}_1, \mathbf{Z}_2, \dots, \mathbf{Z}_V), \mathbf{E} = [\mathbf{E}_1; \mathbf{E}_2; \dots; \mathbf{E}_V],
 \end{aligned} \tag{2}$$

where the term  $\Omega(\cdot)$  merges all self-representation matrices  $\mathbf{Z}_v (v = 1, \dots, V)$  to a third-order tensor  $\mathcal{Z} \in \mathbb{R}^{N \times N \times V}$ ,  $\Phi$  depicts a tensor rank term to explore the relationship of observed samples,  $\Psi$  is another term in accordance with corrupted noise type, and  $\lambda$  is a trade-off parameter to balance the effect of the  $\Phi$  and  $\Psi$  regulations. Usually, sparse noise or outliers will be considered in subspace clustering. Hence, the corresponding convex surrogates  $\ell_1$  or  $\ell_{2,1}$  will be used to remove the sparse noise.

Tucker decomposition [19] and t-SVD [40] are two commonly used tensor approximation methods for MSC. For example, [53] considers Tucker decomposition and its corresponding tensor nuclear norm minimization to extract the low-rank information. Following it, [7] considers simultaneously learning the low-rank Tucker self-representation tensor and the affinity matrix to preserve their correlations. In addition, there are many t-SVD based works with various tensor norms, e.g., standard t-SVD based tensor nuclear norm [49], weighted tensor nuclear norm [11], and weighted tensor Schatten  $p$ -norm [47]. To further enhance the clustering performance,  $\ell_{1,1,2}$  norm term can be added on the self-representation tensor to capture the local correlation in the view dimension [52].

### 3 PROPOSED METHOD

The self-representation tensor obtained from the current MSC works is mainly based on low-rank assumptions, which can explore the global relationship among views. However, the existing works are mainly based on Tucker or t-SVD, which can not fully explore the inter/intra-view information within the self-representation tensor. In this work, we apply low-rank MERA decomposition for MSC, which can adaptively attain a well-explored structure of the self-representation tensor.

#### 3.1 Low-Rank MERA approximation

Low-rank tensor networks have been shown to be more effective in approximating high-order data [2, 27, 42], hence the self-representation tensor  $\mathcal{Z} \in \mathbb{R}^{N \times N \times V}$  is rearranged into a 5th-order tensor  $\mathcal{Y} \in \mathbb{R}^{A \times Q \times A \times Q \times V}$  with  $N = AQ$  for low-rank MERA approximation, while ensuring that  $A$  and  $Q$  are probably close to equilibrium. In this part, we mainly give solutions of low-rank MERA factors for a 5th-order tensor in detail.

Given  $\mathcal{Y} \in \mathbb{R}^{I_1 \times \dots \times I_5}$ , its low-rank MERA approximation is to find MERA factors with predefined MERA ranks  $R_1 = R_2 = R$ , which can be formulated as

$$\min_{\mathcal{U}, \mathcal{W}, \mathbf{B}} \frac{1}{2} \|\mathcal{Y} - f(\mathbf{B}, \mathcal{W}, \mathcal{U})\|_{\mathbb{F}}^2. \quad (3)$$

As shown in Fig. 5, there are four MERA factors including one disentangler  $\mathcal{U}_1$ , two isometries  $\mathcal{W}_1, \mathcal{W}_2$ , and one top core  $\mathbf{B}$ . Each variable can be alternately updated while the others are fixed.

**Update  $\mathcal{U}_1$ :** With fixed  $\mathcal{W}_1, \mathcal{W}_2$ , and  $\mathbf{B}$ , the subproblem of  $\mathcal{U}_1$  can be rewritten into a matrix form as:

$$\min_{\mathbf{U}_1} \frac{1}{2} \|\mathbf{Y}_{(2,3)} - \mathbf{U}_1 \mathbf{M}_u\|_{\mathbb{F}}^2, \text{ s. t. } \mathbf{U}_1^T \mathbf{U}_1 = \mathbf{I}_{I_2 I_3}, \quad (4)$$

where  $\mathbf{Y}_{(2,3)}$  and  $\mathbf{M}_u$  are the mode- $\{2, 3\}$  unfolding matrices of  $\mathcal{Y}$  and  $\mathcal{M}_u$ , respectively.  $\mathcal{M}_u$  is the tensor contraction result of other variables, i.e.,  $\mathcal{M}_u =$

$\mathbf{B} \times_{\{R_1\}} \mathcal{W}_1 \times_{\{R_2\}} \mathcal{W}_2 \in \mathbb{R}^{I_1 \times I_2 \times I_3 \times I_4 \times I_5}$ ;  $\mathbf{U}_1$  is the mode- $\{1, 2\}$  unfolding matrix of  $\mathcal{U}_1 \in \mathbb{R}^{I_2 \times I_3 \times I_2 \times I_3}$ .

The optimization problem (4) is equivalent to the following well-known orthogonal Procrustes problem:

$$\max_{\mathbf{U}_1} \text{trace}((\mathbf{U}_1)^T \mathbf{Y}_{(2,3)} (\mathbf{M}_u)^T), \quad (5)$$

where  $\text{trace}(\mathbf{A})$  calculates the sum of the diagonal elements of  $\mathbf{A}$ , which can be achieved by the Matlab command “trace”. In this way, the updating of  $\mathcal{U}_1$  can be obtained by

$$\mathcal{U}_1 = \text{fold}_{1,2}(\mathbf{S}_u \mathbf{D}_u^T), \quad (6)$$

where  $\mathbf{S}_u$  and  $\mathbf{D}_u$  are the left and right singular vector matrices of the matrix  $\mathbf{Y}_{(2,3)} (\mathbf{M}_u)^T$ .

**Update  $\mathcal{W}_1, \mathcal{W}_2$ :** Following the way of solving  $\mathcal{U}_1$ , the updating of  $\mathcal{W}_p$ ,  $p = 1, 2$  can be obtained by

$$\mathcal{W}_p = \arg \min_{\mathcal{W}_p: \mathbf{W}_p^T \mathbf{W}_p = \mathbf{I}_{R_p}} \frac{1}{2} \|\mathcal{Y} - f(\mathbf{B}, \mathcal{W}, \mathcal{U})\|_{\mathbb{F}}^2. \quad (7)$$

**Update  $\mathbf{B}$ :** The subproblem of  $\mathbf{B}$  can be rewritten as:

$$\min_{\mathbf{B}} \frac{1}{2} \|\mathcal{Y} - \mathcal{C} \times_{\{R_1, R_2\}} \mathbf{B}\|_{\mathbb{F}}^2, \quad (8)$$

where  $\mathcal{C}$  is a 7-th order layer in Definition 3. According to the orthogonal/semi-orthogonal property of disentangler  $\mathcal{U}_1$  and isometries  $\mathcal{W}_p, p = 1, 2$ , the updating of  $\mathbf{B}$  can be obtained by

$$\mathbf{B} = \mathcal{Y} \times_{\{I_1, I_2, I_3, I_4, I_5\}} \mathcal{C}. \quad (9)$$

Repeatedly update equations (6), (7), and (9) for several iterations to achieve low-rank MERA approximation, which is summarized in Algorithm 1.

---

**Algorithm 1** Low-rank MERA approximation

---

- 1: **Input:** 5-th order data  $\mathcal{Y}$ , MERA ranks  $R_1 = R_2 = R$
  - 2: **Initialize:**  $\mathbf{B}, \mathcal{W}, \mathcal{U}$ , Maximum iterations  $S = 10$
  - 3: **for**  $s = 1 : S$  **do**
  - 4:   Update  $\mathcal{U}^s$  via equation (6)
  - 5:   Update  $\mathcal{W}^s$  via equation (7)
  - 6:   Update  $\mathbf{B}^s$  via equation (9)
  - 7: **end for**
  - 8:  $\hat{\mathcal{Y}} = f(\mathbf{B}^S, \mathcal{W}^S, \mathcal{U}^S)$
  - 9: **Output:** Low-rank MERA approximation tensor  $\hat{\mathcal{Y}}$
-



### 3.2 Low-Rank MERA for MSC

As shown in Fig. 2, applying low-rank MERA decomposition on learned self-representation tensor  $\mathcal{Z}$  for MSC can be formulated as the following optimization problem:

$$\begin{aligned} \min_{\{\mathbf{E}_v, \mathbf{Z}_v\}_{v=1}^V} \quad & \sum_{v=1}^V \lambda \|\mathbf{E}_v\|_{2,1} \\ \text{s. t.} \quad & \mathbf{X}_v = \mathbf{X}_v \mathbf{Z}_v + \mathbf{E}_v, v = 1, \dots, V, \\ & \hat{\mathcal{Z}} = f(\mathbf{B}, \mathcal{W}, \mathcal{U}) \end{aligned} \quad (10)$$

where  $\mathcal{Z} = \Omega(\mathbf{Z}_1, \mathbf{Z}_2, \dots, \mathbf{Z}_V) \in \mathbb{R}^{N \times N \times V}$ ,  $\hat{\mathcal{Z}} = \text{reshape}(\mathcal{Z}, [A, Q, A, Q, V])$ . We use operator  $\mathfrak{R}$  to represent these two steps. And  $\mathfrak{R}^{-1}$  denotes its inverse operator.  $\hat{\mathcal{Z}} = f(\mathbf{B}, \mathcal{W}, \mathcal{U})$  means applying low-rank MERA approximation to explore both inter-view and intra-view information.

### 3.3 Solutions

To make the above optimization problem separable, an auxiliary variable  $\mathcal{Y}$  is introduced as follows:

$$\begin{aligned} \min_{\{\mathbf{E}_v, \mathbf{Z}_v\}_{v=1}^V} \quad & \sum_{v=1}^V \lambda \|\mathbf{E}_v\|_{2,1} \\ \text{s. t.} \quad & \mathbf{X}_v = \mathbf{X}_v \mathbf{Z}_v + \mathbf{E}_v, v = 1, \dots, V, \\ & \hat{\mathcal{Z}} = \mathcal{Y}, \mathcal{Y} = f(\mathbf{B}, \mathcal{W}, \mathcal{U}). \end{aligned} \quad (11)$$

The Lagrangian function can be formulated as follows:

$$\begin{aligned} & L(\{\mathbf{Z}_v, \mathbf{E}_v, \Lambda_v\}_{v=1}^V, \mathcal{Y}, \Gamma) \\ & = \sum_{v=1}^V (\lambda \|\mathbf{E}_v\|_{2,1} + \langle \Lambda_v, \mathbf{X}_v - \mathbf{X}_v \mathbf{Z}_v - \mathbf{E}_v \rangle) \\ & + \frac{\mu_2}{2} \|\mathbf{X}_v - \mathbf{X}_v \mathbf{Z}_v - \mathbf{E}_v\|_{\mathbb{F}}^2 + \frac{\mu_1}{2} \|\hat{\mathcal{Z}} - \mathcal{Y}\|_{\mathbb{F}}^2 + \langle \Gamma, \hat{\mathcal{Z}} - \mathcal{Y} \rangle, \end{aligned} \quad (12)$$

under the constraint  $\mathcal{Y} = f(\mathbf{B}, \mathcal{W}, \mathcal{U})$ , where  $\{\Lambda_v\}_{v=1}^V$  and  $\Gamma$  are Lagrangian multipliers and  $\mu_1, \mu_2$  are penalty factors. According to the ADMM framework, problem (12) can be divided into several subproblems where each variable can be alternately updated with other variables fixed.

**Update**  $\{\mathbf{Z}_v\}_{v=1}^V$ : With other variables fixed, the solution of  $\mathbf{Z}_v$  can be obtained by setting the derivative of the objective function in (12) with respect to  $\mathbf{Z}_v$  to zero, as follows:

$$\begin{aligned} & -\mathbf{X}_v^T \Lambda_v - \mu_2 \mathbf{X}_v^T (\mathbf{X}_v - \mathbf{X}_v \mathbf{Z}_v - \mathbf{E}_v) \\ & + \mu_1 (\mathfrak{R}_v^{-1}(\hat{\mathcal{Z}} - \mathcal{Y}) + \mathfrak{R}_v^{-1}(\Gamma)) = \mathbf{0}, \end{aligned} \quad (13)$$

where  $\mathfrak{R}_v^{-1}$  is the inverse operator along the  $v$ -th view, i.e.,  $\mathfrak{R}_v^{-1}(\hat{\mathcal{Z}}) = \mathbf{Z}_v$ . The solution of  $\mathbf{Z}_v$  can be rewritten as:

$$\mathbf{Z}_v = (\mu_1 \mathbf{I} + \mu_2 \mathbf{X}_v^T \mathbf{X}_v)^{-1} (\mathbf{X}_v^T \Lambda_v + \mu_2 \mathbf{X}_v^T \mathbf{X}_v - \mu_2 \mathbf{X}_v^T \mathbf{E}_v + \mathfrak{R}_v^{-1}(\mu_1 \mathcal{Y} - \Gamma)). \quad (14)$$

**Update  $\{\mathbf{E}_v\}_{v=1}^V$ :** The solution of  $\mathbf{E}_v$  can be obtained by optimizing

$$\frac{\lambda}{\mu_2} \|\mathbf{E}_v\|_{2,1} + \frac{1}{2} \|\mathbf{E}_v - (\mathbf{X}_v - \mathbf{X}_v \mathbf{Z}_v + (1/\mu_2) \Lambda_v)\|_{\mathbb{F}}^2. \quad (15)$$

Letting  $\mathbf{D} = \mathbf{X}_v - \mathbf{X}_v \mathbf{Z}_v + (1/\mu_2) \Lambda_v$ , and according to [34], we have

$$\mathbf{E}_v(:, n) = \begin{cases} \frac{\|\mathbf{D}(:, n)\|_2 - \frac{\lambda}{\mu_2}}{\|\mathbf{D}(:, n)\|_2} \mathbf{D}(:, n), & \|\mathbf{D}(:, n)\|_2 > \frac{\lambda}{\mu_2} \\ \mathbf{0}, & \text{otherwise,} \end{cases} \quad (16)$$

where  $n = 1 \cdots N$ ,  $N$  is the number of samples.

**Update  $\mathcal{Y}$ :** With respect to  $\mathcal{Y}$ , the problem (12) can be transferred into the following formulation:

$$\begin{aligned} \min_{\mathcal{Y}} \quad & \frac{\mu_1}{2} \left\| \mathcal{Y} - \left( \hat{\mathcal{Z}} + \frac{1}{\mu_1} \Gamma \right) \right\|_{\mathbb{F}}^2 \\ \text{s. t.} \quad & \mathcal{Y} = f(\mathbf{B}, \mathcal{W}, \mathcal{U}). \end{aligned} \quad (17)$$

It can be solved by Algorithm 1, where the input self-representation tensor is  $\hat{\mathcal{Z}} + \frac{1}{\mu_1} \Gamma$ .

**Update Lagrangian multipliers:**

$$\Gamma = \Gamma + \mu_1 (\hat{\mathcal{Z}} - \mathcal{Y}). \quad (18)$$

$$\Lambda_v = \Lambda_v + \mu_2 (\mathbf{X}_v - \mathbf{X}_v \mathbf{Z}_v - \mathbf{E}_v), v = 1, \dots, V. \quad (19)$$

After finishing updating the variables, the affinity matrix of multi-view data can be obtained by  $\mathbf{S} = \frac{1}{V} \sum_{v=1}^V |\mathbf{Z}_v| + |\mathbf{Z}_v^T|$ , which will be used in spectral clustering algorithm [39] for the final clustering result. The optimization processing of MERA-MSC is summarized in algorithm 2. When  $\max_{v,v=1,\dots,V} \|\mathbf{X}_v - \mathbf{X}_v \mathbf{Z}_v^t - \mathbf{E}_v^t\|_{\infty} \leq \varepsilon$  and  $\max_{v,v=1,\dots,V} \|\mathbf{Z}_v^t - \mathbf{Y}_v^t\|_{\infty} \leq \varepsilon$ ,  $\varepsilon = 10^{-6}$ , our algorithm stops.

The computational complexity of the MERA-MSC algorithm for one iteration is summarized in Table 2. Overall, the main computational complexity is  $O(TN^3(V+1))$  where  $T$  is the number of iterations in Algorithm 2.

---

**Algorithm 2** MERA-MSC

---

- 1: **Input:** Multi-view data  $\{\mathbf{X}_v\}_{v=1}^V, \lambda$
  - 2: **Initialize:**  $\mathcal{Y} = \Gamma = 0; \mathbf{Z}_v = \mathbf{E}_v = \Lambda_v = \mathbf{0}, v = 1, \dots, V; \mu_1 = 10^{-4}; \mu_2 = 5^{-4}; \varepsilon = 10^{-6}; \eta = 2; \mu_1^{\max} = \mu_2^{\max} = 10^{10}; t = 1, T = 50$
  - 3: **while**  $t \leq T$  **do**
  - 4:   **for**  $v = 1 : V$  **do**
  - 5:     Update  $\mathbf{Z}_v^t$  via equation (14)
  - 6:     Update  $\mathbf{E}_v^t$  via equation (16)
  - 7:     Update  $\Lambda_v^t$  via equation (19)
  - 8:   **end for**
  - 9:   Update  $\mathcal{Y}^t$  via equation (17)
  - 10:   Update  $\Gamma^t$  by equation (18)
  - 11:    $\mu_1 = \min(\eta\mu_1, \mu_1^{\max}), \mu_2 = \min(\eta\mu_2, \mu_2^{\max});$
  - 12:   Check convergence conditions
  - 13: **end while**
  - 14: Calculate affinity matrix:  $\mathbf{S} = \frac{1}{V} \sum_{v=1}^V |\mathbf{Z}_v| + |\mathbf{Z}_v^T|$
  - 15: Apply spectral clustering algorithm using  $\mathbf{S}$
  - 16: **Output:** Clustering result
- 

TABLE 1 The computational complexity for one iteration, where  $D$ ,  $N$ , and  $V$  are the dimension of features, the number of samples, and views, respectively.

Variables	$\mathbf{Z}_v$	$\mathbf{E}_v$	$\mathcal{Y}$
Complexity	$O(N^3)$	$O(DN^2)$	$O(N^3V)$
Main Complexity	$O(N^3(1 + V))$		

## 4 EXPERIMENTS

### 4.1 Experimental Settings

#### 4.1.1 Multi-view Datasets Description

Five well-known multi-view datasets are chosen to evaluate the effectiveness of MERA-MSC: **Yale**<sup>1</sup> contains 165 samples of 15 clusters, with 11 samples per subject. We choose 3304-dimension(D) LBP, 6750-D Gabor, and 4096-D intensity as 3 views. **MSRC-v5** [44] consists of 210 image samples collected from 7 clusters with 5 views, including 254-D CENT, 24-D CMT, 512-D GIST, 576-D HOG, 256-D LBP. **Extended YaleB**<sup>2</sup> collects 2432 face image samples from 38 individuals, where each one has 64 images. Following [15], we choose the first 10 classes with 3 views, including 1024-D intensity, 1239-D LBP, and 256-D Gabor. Since data points in one subspace are very close to other subspaces, clustering

<sup>1</sup><http://vision.ucsd.edu/content/yale-face-database>

<sup>2</sup><http://vision.ucsd.edu/leekc/ExtYaleDatabase/ExtYaleB.html>

on this dataset can be a challenge [8]. **Notting-Hill** [55] contains 4660 face samples with 5 classes. We choose intensity 2000-D, 3304-D LBP, and 6750-D Gabor as 3 views. Due to the large number of samples, we will downsample it as 2330 samples with 5 classes. **BDGP** [4] contains 2500 samples from 5 classes with 4 views, including 1000-D lateral, 500-D dorsal, 250-D ventral, and 79-D texture.

The statistical information of the above datasets is summarized in Table 2. Note that each self-representation tensor of size  $N \times N \times V$  is rearranged into a 5th-order tensor for low-rank MERA approximation. The last column of Table 2 displays the sizes of the 5th-order self-representation tensors corresponding to different datasets. More information about this rearrangement can be found in Subsection 3.1.

TABLE 2 Statistical information of different multi-view datasets.

Datasets	Samples	Views	Clusters	5-D $(I_1, \dots, I_5)$
Yale	165	3	15	(11,15,15,11,3)
MSRC-v5	210	5	7	(15,14,15,14,5)
Extended YaleB	640	3	10	(32,20,20,32,3)
Notting-Hill	2330	3	5	(233,10,233,10,3)
BDGP	2000	4	5	(50,50,50,50,4)

#### 4.1.2 Compared Clustering Algorithms

In order to compare clustering performance, we select nine state-of-the-art methods including one single-view method: LRR<sub>best</sub> [22], seven self-representation based multi-view methods: multi-view low-rank representation (MLRR) [2021, TCYB] [5], latent multi-view subspace clustering(L-MSC) [2017, CVPR] [54], exclusivity-consistency regularized multi-view subspace clustering (ECMSC) [2017, CVPR] [43], low-rank tensor constrained multi-view subspace clustering (LTMSC) [2015, ICCV] [53], t-SVD based multi-view subspace clustering (t-SVD-MSC) [2018, IJCV] [49], weighted tensor Schatten  $p$ -norm based multi-view subspace clustering (WTSNM) [2021, TCYB] [47], multi-view subspace clustering tailored tensor low-rank representation (MVSC-TLRR) [2021, TCSVT] [15], and one updated tensor based multi-view clustering method: tensorized bipartite graph learning for multi-view clustering (TBGL-MVC) [2022, TPAMI] [45]. All tests are accomplished on a desktop computer with 2.4 GHz Quad-Core Intel Core i5 Processor and 16 GB 2133 MHz LPDDR3 Memory.

#### 4.1.3 Evaluation Metrics

Six standard evaluation metrics are considered to evaluate the performance in our experiments, including F-score, Precision, Recall, normalized mutual infor-

mation (NMI), adjusted rand index (ARI), and accuracy (ACC). The larger values of these metrics indicate better clustering performance. The detailed information can refer to [30].

#### 4.1.4 Parameter settings

Our MERA-MS-C has two free parameters, one for MERA decomposition, namely MERA rank  $R$ , and the other is the balancing parameter  $\lambda$ . We fix one and tune the other via brute force search. For example, we first fix  $\lambda = 0.01$  and tune parameters  $R$  on the Yale dataset, where  $R$  varies from  $\{4, 8, 12, 16, 20, 24, 28\}$ . The clustering results are reported in Fig. 6(a), where the ACC almost approaches 1 and performs stably when  $R$  ranges in  $[4, 8]$ . In addition, we fix  $R = 6$  to choose the parameter  $\lambda$  from  $\{0, 0.0001, 0.01, 0.1, 0.5, 1\}$ . From Fig. 6(b), we can observe the best clustering performance in terms of six metrics is achieved in a wide range of  $\lambda$ , i.e.,  $\lambda \in [0.001, 0.1]$ .

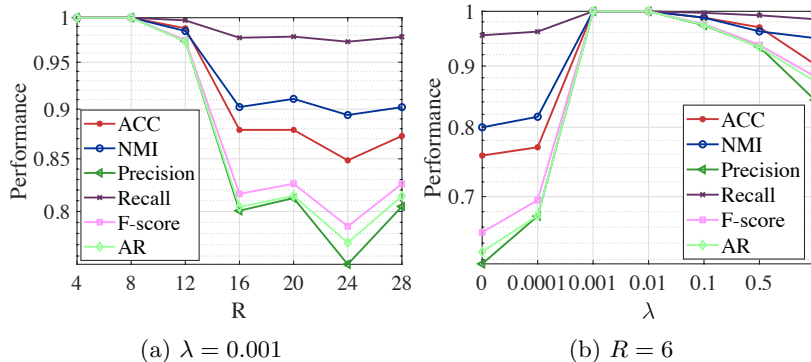


Fig. 6. The change of clustering performance as parameters  $\lambda$  and  $R$  vary. (a)  $R$  changed with  $\lambda = 0.001$ ; (b)  $\lambda$  changed with  $R = 6$ .

## 4.2 Clustering Performance Analysis

Table 3 shows the clustering performance of different methods on five multi-view datasets in terms of F-score, Precision, Recall, AR, NMI, and ACC, where the best and the second best results are highlighted in **bold** and underlined, respectively. For MSRC datasets, several multi-view methods, including WTSNM, MVSC-TLRR, TBGL-MVC, and MERA-MS-C, all reached the best performance with all metrics achieved 1. Meanwhile, our MERA-MS-C also gives the best performance on Yale datasets and outperforms all compared baselines, especially on the extended YaleB dataset. Specifically, our MERA-MS-C provides 2.7% Precision improvement on the Yale dataset; 6.9% NMI improvement on the extended YaleB dataset, 6.6% AR improvement on the Notting Hill dataset, and 0.4% F-score on the BDGP dataset.

Moreover, tensor-based MSC clustering methods, including t-SVD-MSC, WTSNM, MVSC-TLRR and MERA-MSC, generally perform better than matrix-based ones. It verifies the capability of low-rank tensor decomposition to explore high-order correlations from different views. However, considering the extended YaleB dataset, which is hard to cluster due to the effects of high illumination variation; only MVSC-TLRR and the proposed MERA-MSC perform well. Compared to other tensor-based MSC methods, these two methods investigate both inter- and intra-view information throughout the self-representation tensor learning process. The introduction of intra-view information exploration can further enhance the clustering performance. In addition, compared with MVSC-TLRR, our method performs better. This is mainly because low-rank MERA decomposition can adaptively learn both inter-/intra-view from the self-representation tensor and provides a powerful and flexible representation. But for MVSC-TLRR, the contributions from inter-view and intra-view are required to be balanced by weight selection and thus reduce its flexibility.

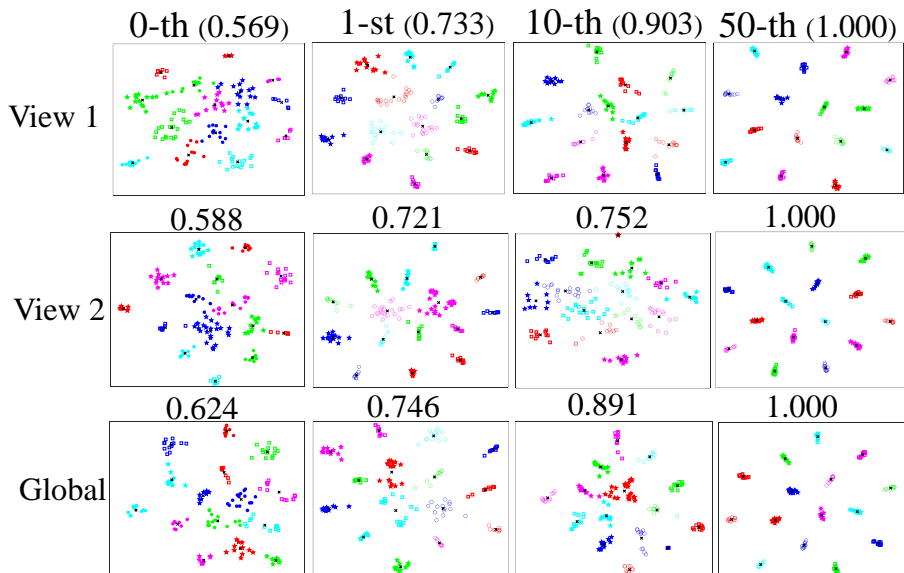


Fig. 7. Visual illustration of latent representation v.s. learning iteration on Yale data, where each feature is visualized by t-SNE [36], and the value indicates the clustering accuracy (ACC) by K-means. View 1 is intensity features; View 2 is LBP features; Global is the fusion features from three different views. The four columns from left to right represent the clustering performance of the 0-th, 1-st, 10-th, and 50-th iterations, respectively.

TABLE 3 Clustering results, e.g., mean value (Standard Deviation) on Yale, MSRC-v5, Extended YaleB, Notting Hill, and BDGP datasets.

Datasets	Methods	F-score	Precision	Recall	NMI	ARI	ACC
MSRC-v5 ( $R=2, \lambda=0.001$ )	LRR-best	0.5469(0.0025)	0.5469(0.0027)	0.5469(0.0027)	0.5658(0.0049)	0.4734(0.0029)	0.6862(0.0015)
	MLRR	0.6674(0.0035)	0.6604(0.0031)	0.6745(0.0031)	0.6828(0.0028)	0.6131(0.0040)	0.7800(0.0038)
	L-MSC	0.6351(0.0074)	0.6197(0.0087)	0.6512(0.0087)	0.6597(0.0086)	0.5745(0.0088)	0.7714(0.0045)
	ECMSC	0.6924(0.0000)	0.6804(0.0000)	0.7048(0.0000)	0.7185(0.0000)	0.6418(0.0000)	0.7857(0.0000)
	LTMSC	0.7148(0.0035)	0.7023(0.0036)	0.7276(0.0036)	0.7444(0.0037)	0.6679(0.0041)	0.8338(0.0027)
	tSVD-MSC	0.9806(0.0000)	0.9803(0.0000)	0.9810(0.0000)	0.9785(0.0000)	0.9775(0.0000)	0.9905(0.0000)
	WTSNM	<b>1.0000(0.0000)</b>	<b>1.0000(0.0000)</b>	<b>1.0000(0.0000)</b>	<b>1.0000(0.0000)</b>	<b>1.0000(0.0000)</b>	<b>1.0000(0.0000)</b>
	MVSC-TLRR	<b>1.0000(0.0000)</b>	<b>1.0000(0.0000)</b>	<b>1.0000(0.0000)</b>	<b>1.0000(0.0000)</b>	<b>1.0000(0.0000)</b>	<b>1.0000(0.0000)</b>
	TBGL-MVC	<b>1.0000(0.0000)</b>	<b>1.0000(0.0000)</b>	<b>1.0000(0.0000)</b>	<b>1.0000(0.0000)</b>	<b>1.0000(0.0000)</b>	<b>1.0000(0.0000)</b>
	MERA-MSC	<b>1.0000(0.0000)</b>	<b>1.0000(0.0000)</b>	<b>1.0000(0.0000)</b>	<b>1.0000(0.0000)</b>	<b>1.0000(0.0000)</b>	<b>1.0000(0.0000)</b>
Yale ( $R=6, \lambda=0.001$ )	LRR-best	0.5483(0.0212)	0.5483(0.0202)	0.5483(0.0202)	0.7111(0.0146)	0.5180(0.0226)	0.7061(0.0146)
	MLRR	0.4884(0.0154)	0.4725(0.0145)	0.5055(0.0145)	0.6569(0.0112)	0.4540(0.0163)	0.6327(0.0192)
	L-MSC	0.5144(0.0096)	0.4689(0.0129)	0.5699(0.0129)	0.7131(0.0058)	0.4796(0.0107)	0.6709(0.0076)
	ECMSC	0.4843(0.0000)	0.4428(0.0000)	0.5345(0.0000)	0.7029(0.0000)	0.4475(0.0000)	0.6545(0.0000)
	LTMSC	0.6005(0.0114)	0.5785(0.0122)	0.6242(0.0122)	0.7500(0.0080)	0.5735(0.0122)	0.7297(0.0042)
	tSVD-MSC	0.9155(0.0657)	0.9037(0.0753)	0.9280(0.0753)	0.9536(0.0364)	0.9099(0.0701)	0.9394(0.0525)
	WTSNM	0.9725(0.0313)	0.9628(0.0504)	0.9833(0.0504)	0.9875(0.0104)	0.9706(0.0335)	0.9800(0.0294)
	MVSC-TLRR	0.9746(0.0000)	0.9734(0.0000)	0.9758(0.0000)	0.9848(0.0000)	0.9729(0.0000)	0.9879(0.0000)
	TBGL-MVC	0.6475(0.0000)	0.5626(0.0000)	0.7624(0.0000)	0.8531(0.0000)	0.6208(0.0000)	0.8606(0.0000)
	MERA-MSC	<b>1.0000(0.0000)</b>	<b>1.0000(0.0000)</b>	<b>1.0000(0.0000)</b>	<b>1.0000(0.0000)</b>	<b>1.0000(0.0000)</b>	<b>1.0000(0.0000)</b>
Extended YaleB ( $R=10, \lambda=1$ )	LRR-best	0.4750(0.0008)	0.4750(0.0007)	0.4750(0.0007)	0.6014(0.0013)	0.4163(0.0009)	0.5827(0.0005)
	MLRR	0.1789(0.0021)	0.1756(0.0023)	0.1822(0.0023)	0.1889(0.0035)	0.0872(0.0025)	0.2561(0.0058)
	L-MSC	0.2791(0.0023)	0.2291(0.0028)	0.3571(0.0028)	0.4453(0.0035)	0.1807(0.0030)	0.4644(0.0010)
	ECMSC	0.3707(0.0000)	0.2841(0.0000)	0.5332(0.0000)	0.6282(0.0000)	0.2777(0.0000)	0.6312(0.0000)
	LTMSC	0.4154(0.0049)	0.4063(0.0055)	0.4250(0.0055)	0.5424(0.0040)	0.3499(0.0056)	0.5109(0.0051)
	tSVD-MSC	0.4584(0.0050)	0.4231(0.0053)	0.5001(0.0053)	0.6113(0.0040)	0.3936(0.0057)	0.6005(0.0028)
	WTSNM	0.4426(0.0043)	0.4070(0.0047)	0.4851(0.0047)	0.5964(0.0033)	0.3757(0.0050)	0.5875(0.0028)
	MVSC-TLRR	0.9139(0.0013)	0.9125(0.0013)	0.9153(0.0013)	0.9123(0.0009)	0.9045(0.0014)	0.9558(0.0008)
	TBGL-MVC	0.2394(0.0000)	0.1560(0.0000)	0.5140(0.0000)	0.4984(0.0000)	0.1038(0.0000)	0.4641(0.0000)
	MERA-MSC	<b>0.9535(0.0000)</b>	<b>0.9497(0.0000)</b>	<b>0.9574(0.0000)</b>	<b>0.9653(0.0000)</b>	<b>0.9484(0.0000)</b>	<b>0.9766(0.0000)</b>
Notting Hill ( $R=15, \lambda=0.0001$ )	LRR-best	0.8047(0.0000)	0.8047(0.0000)	0.8047(0.0000)	0.7456(0.0000)	0.7520(0.0000)	0.8811(0.0000)
	MLRR	0.8394(0.0008)	0.8301(0.0006)	0.8490(0.0006)	0.8006(0.0008)	0.7936(0.0010)	0.8446(0.0007)
	L-MSC	0.7967(0.0000)	0.8033(0.0000)	0.7903(0.0000)	0.8250(0.0000)	0.7402(0.0000)	0.7777(0.0000)
	ECMSC	0.6684(0.0000)	0.5455(0.0000)	0.8627(0.0000)	0.6919(0.0000)	0.5465(0.0000)	0.7300(0.0000)
	LTMSC	0.8320(0.0003)	0.8386(0.0004)	0.8255(0.0004)	0.7949(0.0004)	0.7853(0.0004)	0.9036(0.0002)
	tSVD-MSC	0.8901(0.0000)	0.9096(0.0000)	0.8715(0.0000)	0.8743(0.0000)	0.8601(0.0000)	0.9421(0.0000)
	WTSNM	0.9101(0.0000)	0.9280(0.0000)	0.8929(0.0000)	0.8939(0.0000)	0.8854(0.0000)	0.9532(0.0000)
	MVSC-TLRR	0.8766(0.0000)	0.8929(0.0000)	0.8609(0.0000)	0.8555(0.0000)	0.8427(0.0000)	0.9343(0.0000)
	TBGL-MVC	0.7586(0.0000)	0.7436(0.0000)	0.7742(0.0000)	0.8123(0.0000)	0.6890(0.0000)	0.8476(0.0000)
	MERA-MSC	<b>0.9619(0.0000)</b>	<b>0.9552(0.0000)</b>	<b>0.9687(0.0000)</b>	<b>0.9450(0.0000)</b>	<b>0.9511(0.0000)</b>	<b>0.9700(0.0000)</b>
BDGP ( $R=10, \lambda=0.0002$ )	LRR-best	0.7448(0.0000)	0.7448(0.0000)	0.7448(0.0000)	0.8020(0.0000)	0.6711(0.0000)	0.7004(0.0000)
	MLRR	0.6838(0.0000)	0.6113(0.0000)	0.7758(0.0000)	0.7006(0.0000)	0.5928(0.0000)	0.7064(0.0000)
	L-MSC	0.7354(0.0000)	0.6673(0.0000)	0.8191(0.0000)	0.7762(0.0000)	0.6601(0.0000)	0.6912(0.0000)
	ECMSC	0.7562(0.0000)	0.717(0.0000)	0.800(0.0000)	0.761(0.0000)	0.691(0.0000)	0.789(0.0000)
	LTMSC	0.4325(0.0000)	0.4281(0.0000)	0.4369(0.0000)	0.3889(0.0000)	0.2891(0.0000)	0.5272(0.0000)
	tSVD-MSC	0.9889(0.0000)	0.9888(0.0000)	0.9890(0.0000)	0.9814(0.0000)	0.9861(0.0000)	0.9944(0.0000)
	WTSNM	0.9901(0.0000)	0.9901(0.0000)	0.9911(0.0000)	0.9840(0.0000)	0.9881(0.0000)	0.9951(0.0000)
	MVSC-TLRR	0.9842(0.0000)	0.9841(0.0000)	0.9842(0.0000)	0.9719(0.0000)	0.9802(0.0000)	0.9920(0.0000)
	TBGL-MVC	0.3303(0.0000)	0.2000(0.0000)	0.9487(0.0000)	0.0410(0.0000)	0.0007(0.0000)	0.2236(0.0000)
	MERA-MSC	<b>0.9913(0.0000)</b>	<b>0.9912(0.0000)</b>	<b>0.9913(0.0000)</b>	<b>0.9860(0.0000)</b>	<b>0.9891(0.0000)</b>	<b>0.9956(0.0000)</b>

## 4.3 Discussions

### 4.3.1 Model Analysis

Fig. 7 shows how the clustering performance of the proposed MERA-MSC varies during the learning iteration on the Yale dataset. From the first column of Fig. 7, we can observe the clustering performance on all views is superior to that on a single view. Interestingly, when the low-rank MERA approximation is first used to explore inter/intra-view correlations, the clustering accuracy (ACC) increases by around 11%, as illustrated in the second column of Fig. 7. Iteratively, the correlation within views and across views mutually benefits from the low-rank MERA approximation. This allows us to learn a better latent structure from multi-view data, ultimately achieving a clustering accuracy of 100%. Moreover, the performance improvement indicates that the utilization of information from both within and across views plays a significant role in enhancing clustering accuracy. Additionally, the low-rank MERA approximation effectively explores

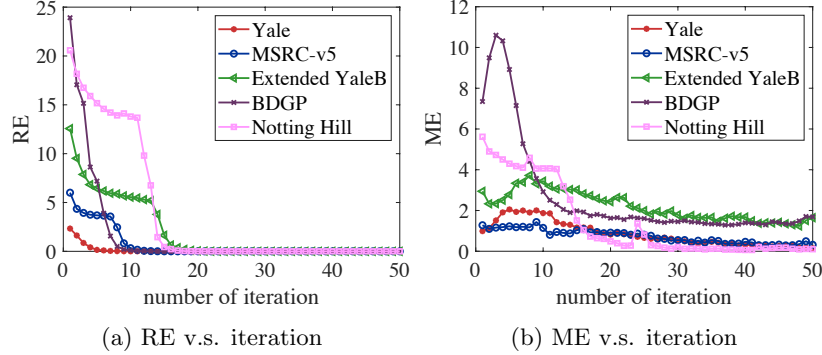


Fig. 8. The convergence performance of MERA-MSC.

the inter-view and intra-view information in the self-representation tensor simultaneously.

#### 4.3.2 Convergence Analysis

Fig. 8 shows the convergence curves of MERA-MSC on different datasets, where the X-axis means the number of iterations and the Y-axis is the values of reconstruction error (RE) and match error (ME), which are defined by  $RE = \max_{v,v=1,\dots,V} \|\mathbf{X}_v - \mathbf{X}_v \mathbf{Z}_v - \mathbf{E}_v\|_\infty$ , and  $ME = \max_{v,v=1,\dots,V} \|\mathbf{Z}_v - \mathbf{Y}_v\|_\infty$ , respectively. It can be observed the RE of MERA-MSC drops very fast at the first 10 iterations and eventually approaches 0 on all datasets. In particular, the larger size of the datasets, the faster the RE and ME change.

#### 4.3.3 Scalability analysis

Most tensor-based MSC methods involve constructing an  $N \times N$  relational graph with a computational complexity of  $O(VN^3)$ , where  $N$  and  $V$  represent the number of instances and views, respectively. This process is time-consuming, particularly for large-scale multi-view data, as the computational time increases with the number of samples.

To extend the MERA-MSC method, we have developed a scalable MERA based multi-view clustering (sMERA-MVC) algorithm. This approach replaces the self-representation learning step, denoted as  $\mathbf{X}_v = \mathbf{X}_v \mathbf{Z}_v + \mathbf{E}_v$ , in the MSC framework (equation (10)), with anchor learning  $\mathbf{X}_v = \mathbf{A}_v \mathbf{C}_v + \mathbf{E}_v$  [33, 41]. The revised framework is illustrated below:

$$\begin{aligned}
 & \min_{\{\mathbf{E}_v, \mathbf{C}_v\}_{v=1}^V} \sum_{v=1}^V \lambda \|\mathbf{E}_v\|_{2,1} \\
 & \text{s. t. } \mathbf{X}_v = \mathbf{A}_v \mathbf{C}_v + \mathbf{E}_v, \mathbf{A}_v^T \mathbf{A}_v = \mathbf{I}_M, v = 1, \dots, V, \\
 & \hat{\mathbf{C}} = f(\mathbf{B}, \mathcal{W}, \mathcal{U}), \hat{\mathbf{C}} = \mathfrak{R}(\mathbf{C}_1, \mathbf{C}_2, \dots, \mathbf{C}_V).
 \end{aligned} \tag{20}$$



TABLE 4 Clustering results on CCV, Caltech-all and ALOI datasets.

Methods	F-score	Precision	Recall	NMI	ARI	ACC	CPU Time (s)
ALOI ( $R=4, \lambda=0.02, M=10$ )							
SMSC	<b>0.7617</b>	<b>0.7129</b>	<u>0.8185</u>	<u>0.8990</u>	<b>0.7591</b>	<b>0.8273</b>	365.7435
LMVSC	0.3874	0.3498	0.4341	0.6964	0.3806	0.4897	93.0113
SMVSC	0.2089	0.1366	0.4437	0.6033	0.1967	0.3251	423.8729
FPMVS-CAG	0.1795	0.1053	0.6062	0.6334	0.1654	0.3121	180.5025
FastMICE	0.6713	<u>0.6223</u>	0.7289	0.8455	0.6678	<u>0.7543</u>	<u>20.3759</u>
sMERA-MVC	<u>0.7130</u>	0.6107	<b>0.8598</b>	<b>0.9114</b>	<u>0.7096</u>	0.7424	<b>19.5916</b>
Caltech-all ( $R=8, \lambda=0.1, M=9$ )							
SMSC	0.1817	0.2935	0.1316	<u>0.4679</u>	0.1671	0.2448	269.1425
LMVSC	0.1685	0.2810	0.1203	0.4374	0.1541	0.2075	92.7087
SMVSC	0.1895	0.1200	<b>0.4496</b>	0.3485	0.1516	<u>0.2906</u>	356.5180
FPMVS-CAG	<u>0.2040</u>	0.1425	<u>0.3589</u>	0.3379	<u>0.1704</u>	0.2654	669.0376
FastMICE	0.1775	<u>0.3209</u>	0.1227	0.4370	0.1644	0.2090	<b>34.8471</b>
sMERA-MVC	<b>0.3807</b>	<b>0.5807</b>	0.2834	<b>0.7533</b>	<b>0.3690</b>	<b>0.4517</b>	<u>56.7210</u>
CCV ( $R=2, \lambda=0.5, M=6$ )							
SMSC	<u>0.1615</u>	<u>0.1599</u>	<u>0.1633</u>	<u>0.2184</u>	<u>0.1096</u>	<u>0.2714</u>	128.4686
LMVSC	0.1202	0.1069	0.1374	0.1694	0.0592	0.2073	59.2433
SMVSC	0.1294	0.1235	0.1359	0.1540	0.0734	0.2110	31.4677
FPMVS-CAG	0.1316	0.1174	0.1496	0.1597	0.0716	0.2282	28.7811
FastMICE	0.1320	0.1387	0.1260	0.1795	0.0816	0.2306	<u>10.3551</u>
sMERA-MVC	<b>0.3603</b>	<b>0.3686</b>	<b>0.3526</b>	<b>0.5087</b>	<b>0.3221</b>	<b>0.4632</b>	<b>6.0318</b>

Here,  $\mathbf{A}_v \in \mathbb{R}^{D_v \times M}$  represents the anchor matrix,  $M$  represents the number of anchors, and  $\mathbf{C}_v \in \mathbb{R}^{M \times N}$  represents the anchor graph. The anchor graph captures the relationships between  $N$  data points and  $M$  anchors (where  $M \ll N$ ) to represent the relationships among all data points, effectively reducing the computational complexity to  $O(VNM^2)$ .  $\hat{\mathbf{C}} = f(\mathbf{B}, \mathcal{W}, \mathcal{U})$  means that low-rank MERA approximation is considered on the anchor graph tensor to well explore the inter/intra-view correlations within multi-view data.

To validate the effectiveness and efficiency of sMERA-MVC, we conducted a comparative analysis with five fast MVC methods on three large-scale datasets. Below, we introduce the datasets used and outline the methods used for comparison.

**Datasets discription:** Amsterdam Library of Object Image (**ALOI**)<sup>3</sup> [12] has a collection of 110250 images of 1000 small objects. Following the approach in [21], we use the first 100 classes as our testing dataset and obtained 10800 samples with four views. Columbia Consumer Video (**CCV**)<sup>4</sup> [16] is a rich database of YouTube videos containing 20 semantic categories. We remove the last 73 samples in our experiment, resulting in 6700 samples. **Caltech-all**<sup>5</sup> [9] has 9144 samples and five views. In our experiment, we remove the last 24

<sup>3</sup><http://elki.dbs.ifi.lmu.de/wiki/DataSets/MultiView>

<sup>4</sup><https://www.ee.columbia.edu/lndvmm/CCV/>

<sup>5</sup>[http://www.vision.caltech.edu/Image Datasets/Caltech101/](http://www.vision.caltech.edu/Image%20Datasets/Caltech101/)

samples to obtain 9120 samples.

**Methods description:** Sparse multi-view spectral clustering (SMSC) [2020, Neurocomputing] [13], large-scale multi-view subspace clustering (LMVSC) [2020, AAAI] [17], scalable multi-view subspace clustering with unified anchors (SMVSC) [2021, ACM MM] [33], fast Parameter-free multiview subspace clustering with consensus anchor guidance (FPMVS-CAG) [2021, TIP] [41], fast multi-view clustering via ensembles (FastMICE) [2023, TKDE] [14].

**Performance and Analysis on Large-Scale Multi-view Datasets:** Table 4 shows the clustering performance of different methods on three large-scale multi-view datasets in terms of F-score, Precision, Recall, AR, NMI, ACC, and CPU time. We can observe that sMERA-MVC consistently outperforms the other five methods regarding clustering performance. In particular, for ALOI, SMSC performs well in most clustering accuracy metrics, with the sMERA-MVC method following closely behind. Notably, sMERA-MVC achieves a significant advantage in terms of CPU time, running approximately 30 times faster than the SMSC. For Caltech-all, sMERA-MVC demonstrates superior performance across all evaluation metrics, except for recall and computation time, surpassing all comparison baselines. Notably, sMERA-MVC excels in all aspects of the CCV dataset, while the performance of the other five methods is comparatively weaker. This further implies that the low-rank MERA approximation exhibits excellent performance in exploring the shared latent structure across views and within individual views in multi-view data.

## 5 CONCLUSION

In this paper, we propose a low-rank MERA based MSC algorithm, where the self-representation tensor can be adaptively learned from the multi-view data and low-rank MERA approximation in each iteration. Benefiting from the interaction among orthogonal/semi-orthogonal factors of low-rank MERA approximation, the correlations present across and within views can be effectively explored. Numerical experiments on five well-known datasets show that MERA-MSC outperforms all state-of-the-art methods in clustering performance evaluated on six different metrics. Besides, we have developed an accelerated and scalable MERA based multi-view clustering algorithm for large-scale multi-view data and verified its effectiveness and efficiency on three large-scale datasets.

## References

- [1] Kim Batselier, Andrzej Cichocki, and Ngai Wong. Meracle: constructive layer-wise conversion of a tensor train into a mera. *Communications on Applied Mathematics and Computation*, 3(2):257–279, 2021.
- [2] Johann A Bengua, Ho N Phien, Hoang Duong Tuan, and Minh N Do. Efficient tensor completion for color image and video recovery: Low-rank tensor train. *TIP*, 26(5):2466–2479, 2017.

- [3] Stephen Boyd, Neal Parikh, Eric Chu, Borja Peleato, Jonathan Eckstein, et al. Distributed optimization and statistical learning via the alternating direction method of multipliers. *Foundations and Trends® in Machine learning*, 3(1):1–122, 2011.
- [4] Xiao Cai, Hua Wang, Heng Huang, and Chris Ding. Joint stage recognition and anatomical annotation of drosophila gene expression patterns. *Bioinformatics*, 28(12):i16–i24, 2012.
- [5] Jie Chen, Shengxiang Yang, Hua Mao, and Conor Fahy. Multiview subspace clustering using low-rank representation. *TCYB*, 2021.
- [6] Yongyong Chen, Shuqin Wang, Xiaolin Xiao, Youfa Liu, Zhongyun Hua, and Yicong Zhou. Self-paced enhanced low-rank tensor kernelized multi-view subspace clustering. *TMM*, 24:4054–4066, 2021.
- [7] Yongyong Chen, Xiaolin Xiao, Chong Peng, Guangming Lu, and Yicong Zhou. Low-rank tensor graph learning for multi-view subspace clustering. *TCSVT*, 2021.
- [8] Ehsan Elhamifar and René Vidal. Sparse subspace clustering: Algorithm, theory, and applications. *TPAMI*, 35(11):2765–2781, 2013.
- [9] Li Fei-Fei, Rob Fergus, and Pietro Perona. Learning generative visual models from few training examples: An incremental bayesian approach tested on 101 object categories. In *CVPRW*, pages 178–178. IEEE, 2004.
- [10] Lele Fu, Zhaoliang Chen, Yongyong Chen, and Shiping Wang. Unified low-rank tensor learning and spectral embedding for multi-view subspace clustering. *TMM*, 2022.
- [11] Quanxue Gao, Wei Xia, Zhizhen Wan, Deyan Xie, and Pu Zhang. Tensor-svd based graph learning for multi-view subspace clustering. In *AAAI*, volume 34, pages 3930–3937, 2020.
- [12] Jan-Mark Geusebroek, Gertjan J Burghouts, and Arnold WM Smeulders. The amsterdam library of object images. *IJCV*, 61:103–112, 2005.
- [13] Zhanxuan Hu, Feiping Nie, Wei Chang, Shuzheng Hao, Rong Wang, and Xuelong Li. Multi-view spectral clustering via sparse graph learning. *Neurocomputing*, 384:1–10, 2020.
- [14] Dong Huang, Chang-Dong Wang, and Jian-Huang Lai. Fast multi-view clustering via ensembles: Towards scalability, superiority, and simplicity. *TKDE*, 2023.
- [15] Yuheng Jia, Hui Liu, Junhui Hou, Sam Kwong, and Qingfu Zhang. Multi-view spectral clustering tailored tensor low-rank representation. *TCSVT*, 31(12):4784–4797, 2021.

- [16] Yu-Gang Jiang, Guangnan Ye, Shih-Fu Chang, Daniel Ellis, and Alexander C. Loui. Consumer video understanding: A benchmark database and an evaluation of human and machine performance. In *ICMR, oral session*, 2011.
- [17] Zhao Kang, Wangtao Zhou, Zhitong Zhao, Junming Shao, Meng Han, and Zenglin Xu. Large-scale multi-view subspace clustering in linear time. In *AAAI*, volume 34, pages 4412–4419, 2020.
- [18] Misha E Kilmer and Carla D Martin. Factorization strategies for third-order tensors. *Linear Algebra and its Applications*, 435(3):641–658, 2011.
- [19] Tamara G Kolda and Brett W Bader. Tensor decompositions and applications. *SIAM review*, 51(3):455–500, 2009.
- [20] Zhenglai Li, Chang Tang, Xinwang Liu, Xiao Zheng, Wei Zhang, and En Zhu. Consensus graph learning for multi-view clustering. *TMM*, 24:2461–2472, 2021.
- [21] Youwei Liang, Dong Huang, Chang-Dong Wang, and S Yu Philip. Multi-view graph learning by joint modeling of consistency and inconsistency. *TNNLS*, 2022.
- [22] Guangcan Liu, Zhouchen Lin, Shuicheng Yan, Ju Sun, Yong Yu, and Yi Ma. Robust recovery of subspace structures by low-rank representation. *TPAMI*, 35(1):171–184, 2012.
- [23] Ji Liu, Przemyslaw Musialski, Peter Wonka, and Jieping Ye. Tensor completion for estimating missing values in visual data. *TPAMI*, 35(1):208–220, 2012.
- [24] Yipeng Liu. *Tensors for Data Processing: Theory, Methods, and Applications*. Academic Press, 2022.
- [25] Yipeng Liu, Longxi Chen, and Ce Zhu. Improved robust tensor principal component analysis via low-rank core matrix. *JSTSP*, 12(6):1378–1389, 2018.
- [26] Yipeng Liu, Jiani Liu, Zhen Long, and Ce Zhu. *Tensor computation for data analysis*. Springer, 2022.
- [27] Zhen Long, Ce Zhu, Jiani Liu, and Yipeng Liu. Bayesian low rank tensor ring for image recovery. *TIP*, 30:3568–3580, 2021.
- [28] Shirui Luo, Changqing Zhang, Wei Zhang, and Xiaochun Cao. Consistent and specific multi-view subspace clustering. In *AAAI*, volume 32, 2018.
- [29] Yazhou Ren, Ni Wang, Mingxia Li, and Zenglin Xu. Deep density-based image clustering. *Knowledge-Based Systems*, 197:105841, 2020.

- [30] Hinrich Schütze, Christopher D Manning, and Prabhakar Raghavan. *Introduction to information retrieval*, volume 39. Cambridge University Press Cambridge, 2008.
- [31] Xiaochuang Shu, Xiangdong Zhang, Quanxue Gao, Ming Yang, Rong Wang, and Xinbo Gao. Self-weighted anchor graph learning for multi-view clustering. *TMM*, 2022.
- [32] Xiaomeng Si, Qiyue Yin, Xiaojie Zhao, and Li Yao. Consistent and diverse multi-view subspace clustering with structure constraint. *PR*, 121:108196, 2022.
- [33] Mengjing Sun, Pei Zhang, Siwei Wang, Sihang Zhou, Wenxuan Tu, Xinwang Liu, En Zhu, and Changjian Wang. Scalable multi-view subspace clustering with unified anchors. In *Multimedia*, pages 3528–3536, 2021.
- [34] Chang Tang, Xinzhong Zhu, Xinwang Liu, Miaomiao Li, Pichao Wang, Changqing Zhang, and Lizhe Wang. Learning a joint affinity graph for multiview subspace clustering. *TMM*, 21(7):1724–1736, 2018.
- [35] Yongqiang Tang, Yuan Xie, Chenyang Zhang, and Wensheng Zhang. Constrained tensor representation learning for multi-view semi-supervised subspace clustering. *TMM*, 24:3920–3933, 2021.
- [36] Laurens Van der Maaten and Geoffrey Hinton. Visualizing data using t-sne. *JMLR*, 9(11), 2008.
- [37] Guifré Vidal. Class of quantum many-body states that can be efficiently simulated. *Physical Review Letters*, 101(11):110501, 2008.
- [38] René Vidal and Paolo Favaro. Low rank subspace clustering (lrsc). *Pattern Recognition Letters*, 43:47–61, 2014.
- [39] Ulrike Von Luxburg. A tutorial on spectral clustering. *Statistics and computing*, 17(4):395–416, 2007.
- [40] Shuqin Wang, Yongyong Chen, Yigang Ce, Linna Zhang, and Viacheslav Voronin. Low-rank and sparse tensor representation for multi-view subspace clustering. In *ICIP*, pages 1534–1538. IEEE, 2021.
- [41] Siwei Wang, Xinwang Liu, Xinzhong Zhu, Pei Zhang, Yi Zhang, Feng Gao, and En Zhu. Fast parameter-free multi-view subspace clustering with consensus anchor guidance. *TIP*, 31:556–568, 2021.
- [42] Wenqi Wang, Vaneet Aggarwal, and Shuchin Aeron. Efficient low rank tensor ring completion. In *ICCV*, pages 5697–5705, 2017.
- [43] Xiaobo Wang, Xiaojie Guo, Zhen Lei, Changqing Zhang, and Stan Z Li. Exclusivity-consistency regularized multi-view subspace clustering. In *CVPR*, pages 923–931, 2017.

- [44] John Winn and Nebojsa Jojic. Locus: Learning object classes with unsupervised segmentation. In *ICCV*, volume 1, pages 756–763. IEEE, 2005.
- [45] Wei Xia, Quanxue Gao, Qianqian Wang, Xinbo Gao, Chris Ding, and Dacheng Tao. Tensorized bipartite graph learning for multi-view clustering. *TPAMI*, 2022.
- [46] Wei Xia, Qianqian Wang, Quanxue Gao, Xiangdong Zhang, and Xinbo Gao. Self-supervised graph convolutional network for multi-view clustering. *TMM*, 24:3182–3192, 2021.
- [47] Wei Xia, Xiangdong Zhang, Quanxue Gao, Xiaochuang Shu, Jungong Han, and Xinbo Gao. Multiview subspace clustering by an enhanced tensor nuclear norm. *TCYB*, 2021.
- [48] Xiaolin Xiao, Yue-Jiao Gong, Zhongyun Hua, and Wei-Neng Chen. On reliable multi-view affinity learning for subspace clustering. *TMM*, 23:4555–4566, 2020.
- [49] Yuan Xie, Dacheng Tao, Wensheng Zhang, Yan Liu, Lei Zhang, and Yanyun Qu. On unifying multi-view self-representations for clustering by tensor multi-rank minimization. *IJCV*, 126(11):1157–1179, 2018.
- [50] Jie Xu, Chao Li, Liang Peng, Yazhou Ren, Xiaoshuang Shi, Heng Tao Shen, and Xiaofeng Zhu. Adaptive feature projection with distribution alignment for deep incomplete multi-view clustering. *TIP*, 32:1354–1366, 2023.
- [51] Ke Ye and Lek-Heng Lim. Tensor network ranks. *arXiv preprint arXiv:1801.02662*, 2018.
- [52] Ming Yin, Junbin Gao, Shengli Xie, and Yi Guo. Multiview subspace clustering via tensorial t-product representation. *TNNLS*, 30(3):851–864, 2018.
- [53] Changqing Zhang, Huazhu Fu, Si Liu, Guangcan Liu, and Xiaochun Cao. Low-rank tensor constrained multiview subspace clustering. In *ICCV*, pages 1582–1590, 2015.
- [54] Changqing Zhang, Qinghua Hu, Huazhu Fu, Pengfei Zhu, and Xiaochun Cao. Latent multi-view subspace clustering. In *CVPR*, pages 4279–4287, 2017.
- [55] Yi-Fan Zhang, Changsheng Xu, Hanqing Lu, and Yeh-Min Huang. Character identification in feature-length films using global face-name matching. *TMM*, 11(7):1276–1288, 2009.
- [56] Shuai Zheng, Xiao Cai, Chris Ding, Feiping Nie, and Heng Huang. A closed form solution to multi-view low-rank regression. In *AAAI*, 2015.
- [57] Tao Zhou, Changqing Zhang, Xi Peng, Harish Bhaskar, and Jie Yang. Dual shared-specific multiview subspace clustering. *TCYB*, 50(8):3517–3530, 2019.